



Cite this: *Phys. Chem. Chem. Phys.*,  
2018, 20, 25693

Received 12th June 2018,  
Accepted 20th September 2018

DOI: 10.1039/c8cp03726d

rsc.li/pccp

# Effects of thermal disorder on the electronic structure of halide perovskites: insights from MD simulations

Marko Mladenović† and Nenad Vukmirović \*

The effects of thermal disorder on the electronic properties of organic/inorganic halide perovskites were investigated using *ab initio* molecular dynamics simulations. It was generally found that band gap variations due to effects of thermal disorder are the largest in materials with the smallest lattice constant. The factors that may lead to departure from this trend include the degree of rotational and translational motion of the organic cation and the strength of its dipole. It was found that the contribution of the flexible organic part to the band gap variations is considerably smaller than the contribution of the inorganic part of the material. The results of our simulations indicate that band gap variations in halide perovskites fall within the range exhibited in inorganic semiconductors.

## 1 Introduction

Organic/inorganic halide perovskite materials have attracted enormous attention in the last several years due to their outstanding optoelectronic properties.<sup>1,2</sup> In particular, these materials can be used as low-cost active materials in solar cells<sup>3,4</sup> with power conversion efficiencies larger than 20%.<sup>5</sup> As a consequence, there is a strong interest in understanding their electronic properties and the factors that affect them.

The chemical formula of hybrid perovskites is  $ABX_3$ , where A is the organic cation (for example  $CH_3NH_3^+$ ,  $HC(NH_2)_2^+$ ,  $NH_4^+$ ), B is the metal cation (for example  $Pb^{2+}$ ,  $Sn^{2+}$ ) and X is the halide anion ( $Cl^-$ ,  $Br^-$ ,  $I^-$ ). It is by now well established that the highest states in the valence band and lowest states in the conduction band originate from orbitals of inorganic elements.<sup>6–13</sup> On the other hand, there is a wealth of evidence that organic cations have significant rotational freedom, especially at room temperature or higher temperatures.<sup>14–35</sup> Consequently, a single material combines a flexible organic part with a more inert inorganic part.

The flexibility of organic semiconductors has a profound effect on their electronic properties. Displacements of atoms at room temperature are large enough to lead to variations of the energies of the highest occupied and lowest unoccupied states comparable to the bandwidths. This effect, termed as dynamic

or thermal disorder, often leads to localization of charge carriers, and strongly affects the electrical transport properties.<sup>36–46</sup> While it is a significant challenge to reliably calculate the charge carrier mobility in thermally disordered materials,<sup>47</sup> it is generally understood that stronger thermal disorder leads to smaller charge carrier mobility. On the other hand, in the case of inorganic semiconductors atomic displacements have a weaker effect and can be usually treated perturbatively as electron-phonon interactions.<sup>48,49</sup>

The main goal of this work is to understand the effect of thermal disorder on the electronic properties of several of the most widely used organic/inorganic halide perovskite materials. We investigate these effects using *ab initio* molecular dynamics (MD) simulations at finite temperature by tracking the evolution of the conduction and valence band edge energies as a function of time. Stronger variations of band edge energies produce a more disordered potential for charge carriers and consequently lead to smaller charge carrier mobility. To quantify this effect caused by thermal disorder using a single parameter, we calculate the standard deviation of the band gap during the evolution of the system. It is expected that larger standard deviation of the band gap will lead to slower electrical transport.

We compare the effects of different cations by keeping lead-iodide ( $PbI_3$ ) as the inorganic part and replacing the organic cation methylammonium (MA,  $CH_3NH_3^+$ ) with formamidinium (FA,  $HC(NH_2)_2^+$ ) and ammonium ( $NH_4^+$ ). Additionally, we investigate the effects of metal and halide atom substitution by replacing Pb with Sn and I with Br and Cl while keeping MA as a cation. To isolate the effects of the organic part of the material we perform two sets of simulations – in one set the atoms in the inorganic part are fixed, while in the other set all atoms are allowed to move.

Scientific Computing Laboratory, Center for the Study of Complex Systems,  
Institute of Physics Belgrade, University of Belgrade, Pregrevica 118,  
11080 Belgrade, Serbia. E-mail: nenad.vukmirovic@iph.ac.rs

† Present address: Laboratory of Computational Chemistry and Biochemistry,  
Institute of Chemical Sciences and Engineering, École Polytechnique Fédérale de  
Lausanne, CH-1015 Lausanne, Switzerland.

While *ab initio* molecular dynamics was extensively used in recent years to study the properties of perovskite materials,<sup>14,15,18,20,22–28,30,50</sup> very few of these studies have analyzed the effects of atomic motion on band edge energies and energy gap<sup>14,20,23</sup> and these studies were focused on a single or two perovskite materials. In ref. 14 the authors reported the variations of the HOMO energies of cubic MAPbI<sub>3</sub> at temperatures of 268 K and 319 K (which are below the tetragonal to cubic phase transition and represent hypothetical undercooled cubic structures) and found that the standard deviation of these variations is respectively 54 and 78 meV. In ref. 20 the authors presented the results of band gap variations for MAPbI<sub>3</sub> in three different tetragonal phases and FAPbI<sub>3</sub> in the cubic phase at a temperature of 350 K. They obtained standard deviation of the band gap in the range from 15 to 40 meV. In ref. 23, a tetragonal phase of MAPbI<sub>3</sub> at a temperature of 220 K was analyzed and a band gap standard deviation of 90 meV was obtained. Other *ab initio* MD studies were focused on different effects or properties, such as temporal behavior of the cation orientation and positions,<sup>15,18,24,25,27</sup> the phase transition between the tetragonal and cubic phase,<sup>22,28</sup> (anti)ferroelectric ordering of molecular dipoles,<sup>26,30</sup> and the effects of material degradation by water.<sup>50</sup>

In this work, we analyze the effects of thermal disorder on the electronic structure in detail for a class of organic/inorganic halide perovskite materials and establish and interpret the trends obtained with substitution of a metal atom, halide atom or organic group. We find that the variations of the band gap when all atoms are allowed to move are somewhat smaller than those in inorganic polar semiconductor GaAs and significantly larger than those in Si. Variations in the band gap are highest in perovskites with Br and Cl halide atoms and the smallest in perovskites with ammonium as an organic cation. In the case of a fixed inorganic part, the variations in the band gaps become considerably smaller. We discuss the factors responsible for such trends and the implications for material properties.

## 2 Computational methodology

To investigate the effects of thermal disorder on the electronic structure of halide perovskites, we used *ab initio* Born–Oppenheimer MD simulations. The simulations were performed using the Quantum ESPRESSO package.<sup>51,52</sup> Two sets of MD simulations were carried out: (1) simulations without any constraints for atomic positions and lattice parameters and (2) simulations where only the organic cation is allowed to move freely. Starting geometries for all investigated perovskites were  $2 \times 2 \times 2$  pseudocubic supercells, each containing 8 stoichiometric units, with lattice parameters listed in Table 1. Most of the lattice parameters are taken from ref. 53, which is the database of lattice parameters used in several theoretical studies.<sup>18,54,55</sup> Lattice parameters for the initial structure of MASnI<sub>3</sub> are taken from ref. 56. We note that a single unit cell of perovskites with an organic group is not strictly cubic since orientation of the organic cation defines a preferential direction in space and slightly distorts the cubic shape of the cell. In real materials

Table 1 Pseudocubic unit cell parameters for the initial structure of the perovskites investigated in this work

	<i>a</i> (Å)	<i>b</i> (Å)	<i>c</i> (Å)
MAPbI <sub>3</sub> <sup>53</sup>	6.29	6.27	6.30
MAPbBr <sub>3</sub> <sup>53</sup>	5.92	5.92	5.92
MAPbCl <sub>3</sub> <sup>53</sup>	5.68	5.68	5.68
MASnI <sub>3</sub> <sup>56</sup>	6.23	6.23	6.23
FAPbI <sub>3</sub> <sup>53</sup>	6.41	6.27	6.34
NH <sub>4</sub> PbI <sub>3</sub> <sup>53</sup>	6.21	6.21	6.21

different orientations of organic cations in different cells lead to a cubic structure on average. The distortion of the cubic cell is only slight in most materials, as can be seen in Table 1. Nevertheless, we refer to these cells that are used in our initial structure as pseudocubic. We used norm-conserving pseudo-potentials with kinetic energy cut-off 60 Ry,  $2 \times 2 \times 2$   $\Gamma$ -point centered reciprocal points grid and local density approximation (LDA) for exchange–correlation potential. To estimate the accuracy of LDA for quantities of interest in this work, additional calculations using other levels of theory were also performed. In a set of these calculations, we used the hybrid PBE0 functional<sup>57,58</sup> with the effects of spin–orbit interaction taken into account. In another set of calculations, we included the semi-empirical DFT-D dispersion correction<sup>59</sup> in the functional.

The temperature was set to  $T = 350$  K in all simulations and it was controlled *via* velocity rescaling. This temperature was used to enable a fair comparison between the investigated materials since all investigated perovskites with MA as an organic cation exhibit a cubic structure at this temperature.<sup>2,56,60,61</sup> On the other hand, at room temperature, MAPbI<sub>3</sub> adopts a tetragonal phase.<sup>21,62</sup> For FAPbI<sub>3</sub>, both cubic<sup>18</sup> and trigonal<sup>56</sup> structures are reported, whereas for NH<sub>4</sub>PbI<sub>3</sub> there is no experimental evidence of the structure and theoretical studies assume a cubic structure.<sup>54</sup>

MD simulations consisted of a 2 ps long equilibration run followed by an 8 ps long production run. This time is larger than the time necessary for organic cation rotation which was estimated to be on the order of a picosecond.<sup>14,17,19,27,63</sup> Consequently, the organic cation can exhibit a variety of different orientations during this time and it is expected that this timescale is representative enough to reliably estimate the effects of thermal disorder. The simulations without constraints on atomic coordinates were performed at constant temperature and pressure, which implies variable cell dimensions, while simulations with fixed inorganic parts were performed at constant temperature and volume, which implies fixed cell dimensions. The time dependence of the simulated Kohn–Sham band gap of halide perovskite materials investigated in this work is presented in Fig. 1. As can be seen from the figure, for some materials the band gap exhibits strong variations during the first 2 ps of MD simulation due to system equilibration. Consequently, the first 2 ps of each MD simulation were excluded from the analysis.

Next, we discuss possible effects of limited supercell size on the results. Several previous *ab initio* MD simulations of halide perovskites<sup>14,20,64</sup> were performed using the  $2 \times 2 \times 2$  supercell

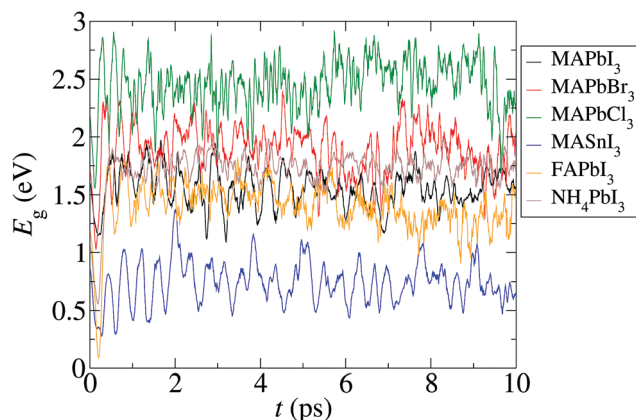


Fig. 1 Time evolution of the simulated Kohn–Sham band gap of halide perovskite materials investigated in this work.

and simulation time on the order of 10 ps, while longer simulation times and larger supercells were employed in more recent studies.<sup>15,24,26,28</sup> It was pointed out in ref. 15 that the limited supercell size may lead to a reduced decay of the dipole autocorrelation function in the case of tetragonal MAPbI<sub>3</sub> at room temperature. On the other hand, in ref. 26 nearly the same distribution of organic cation orientation was obtained in the simulations with a  $2 \times 2 \times 2$  supercell as in the simulations with  $4 \times 4 \times 4$  and  $6 \times 6 \times 6$  supercells, while the dipole autocorrelation functions are largely similar. Nearly the same dipole autocorrelation function was obtained in ref. 24 from  $2 \times 2 \times 2$  and  $4 \times 4 \times 4$  supercells for MAPbI<sub>3</sub> at a temperature of 400 K. Consequently, we choose the  $2 \times 2 \times 2$  supercell as a compromise between computational cost and accuracy. Since the main focus of our study is on comparison between similar materials, we believe that any possible systematic errors arising from limited supercell dimensions would be nearly the same in similar materials.

### 3 Results and discussion

Calculated band gaps and their standard deviations are summarized in Table 2. Band gaps and the corresponding standard deviations were calculated as average of the values obtained at different MD steps. Calculated values for the MAPbI<sub>3</sub> and FAPbI<sub>3</sub> band gaps are within the range of reported experimental values (1.5–1.6 eV for MAPbI<sub>3</sub><sup>22,65</sup> and 1.4–1.5 eV for FAPbI<sub>3</sub><sup>56,66</sup>). In the case of NH<sub>4</sub>PbI<sub>3</sub>, our band gap of 1.75 eV is higher than the

Table 2 Average values of band gaps ( $E_g$ ) and standard deviations of band gaps in MD simulation without constraints ( $\sigma(E_g)$ ) and in MD simulation with a fixed inorganic part ( $\sigma_r(E_g)$ ) for the studied perovskite materials

	$E_g$ (eV)	$\sigma(E_g)$ (eV)	$\sigma_r(E_g)$ (eV)
MAPbI <sub>3</sub>	1.54	0.15	0.079
MAPbBr <sub>3</sub>	1.90	0.19	0.059
MAPbCl <sub>3</sub>	2.47	0.19	0.079
MASnI <sub>3</sub>	0.76	0.16	0.052
FAPbI <sub>3</sub>	1.41	0.15	0.032
NH <sub>4</sub> PbI <sub>3</sub>	1.75	0.088	0.054

reported band gap of 1.13 eV calculated using the LDA functional.<sup>55</sup> This difference originates from the fact that the gap in ref. 55 was calculated for a fixed cubic structure, while in our simulation the structure becomes distorted, which, on average, decreases the antibonding overlap between the Pb and I atoms and increases the band gap. A similar observation related to the structure of NH<sub>4</sub>PbI<sub>3</sub> was reported in ref. 11. However, one should bear in mind that there is no experimental evidence of perovskite phase of NH<sub>4</sub>PbI<sub>3</sub> and we use this compound just for comparison with MAPbI<sub>3</sub> and FAPbI<sub>3</sub>. For other compounds our band gaps are lower than the experimental values (around 2.2 eV for MAPbBr<sub>3</sub>,<sup>65</sup> around 3 eV for MAPbCl<sub>3</sub><sup>65</sup> and around 1.3 eV for MASnI<sub>3</sub><sup>56</sup>) expressing the well-known problem of LDA band gap underestimation. In the case of PbI<sub>3</sub> perovskites, LDA (and other local functionals such as PBE) gives good estimates for band gaps due to the cancellation of the LDA error and the error of spin–orbit coupling effect neglect.<sup>67</sup> However, the goal of this work is to estimate the effects of thermal disorder on the electronic properties of the material and the focus was not on calculation of correct absolute values of band gaps.

To check the accuracy of LDA in quantifying the degree of variations of the band gap, we have performed electronic structure calculations for 9 snapshots from the MD trajectory, taken at  $t = 2, 3, \dots, 10$  ps, in the case of the MAPbI<sub>3</sub> and MASnI<sub>3</sub> material, using the hybrid PBE0 functional with the effects of spin–orbit interaction (PBE0 + SOC), which we used because it is known to give a rather accurate band structure of halide perovskites.<sup>68</sup> In the case of MAPbI<sub>3</sub>, the standard deviation of the band gap estimated from these snapshots is 158 meV for PBE0 + SOC calculations, while it is 138 meV for LDA calculations. For the MASnI<sub>3</sub> material, the standard deviation calculated from selected snapshots (8 snapshots taken at  $t = 3, 4, \dots, 10$  ps were selected because their standard deviation of the band gap is very similar to full production trajectory) is 174 meV in PBE0 + SOC calculation and 154 meV in LDA calculation. These results suggest that LDA gives rather similar values of standard deviations of the band gap to the more accurate functional.

Another known deficiency of local functionals such as LDA is the inability to treat dispersion interactions.<sup>69</sup> The role of dispersion interactions in organic/inorganic halide perovskites was discussed in some recent studies.<sup>70,71</sup> To assess their role when band gap variations are concerned, we have performed additional MD simulations where dispersion correction<sup>59</sup> was included in the functional. These simulations were performed for MAPbI<sub>3</sub> and FAPbI<sub>3</sub> materials which contain different organic groups and consequently significantly different dispersion interaction between the organic group and the inorganic cage. In such simulations, we find that the standard deviation of the band gap is 152 meV for MAPbI<sub>3</sub> and 167 meV for FAPbI<sub>3</sub>. Therefore, these results only slightly differ from the values obtained in the simulation based on LDA (146 meV for MAPbI<sub>3</sub> and 154 meV for FAPbI<sub>3</sub>, see Table 2), suggesting that dispersion interactions have only a minor effect on the results reported in this work. A similar conclusion was obtained also in ref. 23 where the same band gap variations of tetragonal MAPbI<sub>3</sub> were

obtained in simulations with a local functional and with a dispersion-corrected functional.

Values for standard deviations of band gaps in the case of MD simulations without any constraints are significant. They are all within the range of (0.14–0.20) eV, except for  $\text{NH}_4\text{PbI}_3$  which has a smaller standard deviation. We note that our results yield larger values than previous similar studies of  $\text{MAPbI}_3$ . This is to a large extent expected since the work in ref. 23 considered tetragonal  $\text{MAPbI}_3$  at a low temperature of 220 K, while the simulations in ref. 14 and 20 were performed with fixed Pb atoms and fixed unit cell. To compare the values that we obtained with the corresponding values in inorganic semiconductors, we also performed MD simulations of conventional inorganic semiconductors Si and GaAs. The values that we obtained for perovskites are somewhat smaller than that for inorganic polar semiconductor GaAs that has a standard deviation of the band gap of 0.30 eV, but are significantly larger than those of Si where the standard deviation is only 34 meV.

Next, we also discuss variations of individual conduction band minimum (CBM) and valence band maximum (VBM) energies. In the simulation with a fixed inorganic part (and with fixed supercell), we find for all materials that the standard deviations of the CBM and VBM are rather similar ( $\sigma_f^{\text{CBM}} \approx \sigma_f^{\text{VBM}}$ ) and that these are approximately equal to  $\sigma_f(E_g)/\sqrt{2}$ . Such results suggest that one can consider the total band gap variation  $\sigma_f(E_g)$  to be composed of equal contributions from CBM and VBM satisfying  $(\sigma_f^{\text{CBM}})^2 + (\sigma_f^{\text{VBM}})^2 = \sigma_f(E_g)^2$ . For these reasons, throughout the paper we report only the total band gap variation. On the other hand, within the current simulation setup it is not possible to check if the same relations hold in the simulation without any constraints when supercell dimensions also vary. The reason for this is that the VBM and CBM values obtained from different supercells have different reference energies.

To understand the trends in standard deviations of the band gaps among different perovskite materials, we first discuss different factors that lead to these variations. Since the highest states in the valence band and lowest states in the conduction band originate from the inorganic part, thermal disorder directly influences the band gap by modulating the transfer integrals between relevant orbitals of metal and halide atoms and consequently modulates the band gap of the material. This is the same mechanism as in inorganic semiconductors. On the other hand, organic cations create electrical potential that varies with time and consequently modulates the energies of orbitals of inorganic atoms, leading also to modulation of the band gap. The following factors influence the strength of these variations: (a) lattice constant of the material. For smaller lattice constants, the organic cation is closer to the inorganic atoms leading to stronger variations of the value of electrical potential on the inorganic atoms. (b) The strength of the organic cation dipole. Larger dipole moment of the organic cation leads to larger variations of electrical potential on the inorganic atoms. The MA cation has the largest dipole moment of 2.2 D, and the dipole moment of FA is around 0.2 D, while ammonium cation has no dipole moment.<sup>21</sup> (c) Rotational

flexibility of the organic cations. If the organic cation has more freedom to rotate, its dipole moment can be oriented in many different directions, leading to stronger variations in the potential it creates. (d) Translational motion flexibility of the organic cation. If there is enough space for the organic cation to move as a whole, its charge will create stronger variations of the potential. A quantitative measure of the factor (a) is simply the value of the lattice constant and the measure of the factor (b) is the dipole moment of the organic cation. To quantify the factor (c) we use the conformational entropy defined as

$$s = - \int_0^\pi \sin \theta \, d\theta \int_0^{2\pi} d\phi f(\theta, \phi) \ln \left[ \frac{f(\theta, \phi)}{f_0} \right]. \quad (1)$$

In eqn (1), the variables  $\theta$  and  $\phi$  denote polar and azimuthal angle that represent the direction of the orientation of the cation, while  $f(\theta, \phi)$  is the probability density describing the probability of orientation of the dipole in different directions and  $f_0 = 1 \text{ rad}^{-2}$ .  $f(\theta, \phi)$  is normalized to satisfy  $\int_0^\pi \sin \theta \, d\theta \int_0^{2\pi} d\phi f(\theta, \phi) = 1$ . To quantify the factor (d) we follow the position of the middle of the C–N bond for MA based perovskites, the position of the C atom for FA based perovskites and the position of the N atom for ammonium based materials. Then, we use mean square displacement of this position to quantify the flexibility of organic cation translational motion.

The results obtained for standard deviations of the band gap are presented in Table 2. We first discuss the results of the full simulation when there are no constraints on the lattice parameters or the motion of atoms. The overall trend is that variations tend to decrease with an increase in the lattice constant of the material, as can be seen in Fig. 2. This effect is expected since for a smaller lattice constant the influence of the organic cations on the band gap variations is stronger [the factor (a) discussed in the previous paragraph]. However, effects other than the lattice constant may lead to departures from the main trend. The most pronounced departure occurs in

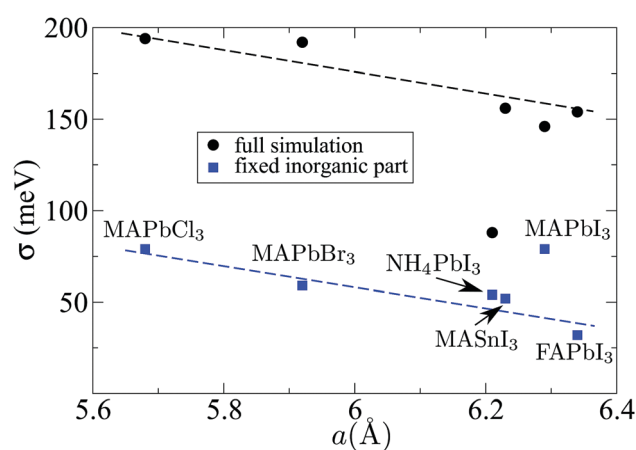
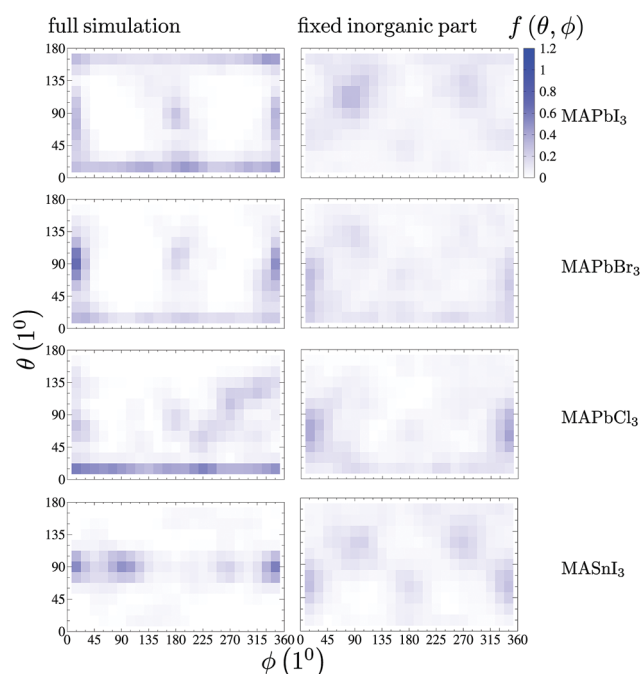


Fig. 2 Dependence of the standard deviation of the band gap on the lattice constant in the case of the simulation without any constraints (circles) and the simulation with a fixed inorganic part (squares). Dashed lines are given only as a guide to the eye.

**Table 3** Rotational entropy and mean square displacement of translational motion in MD simulation without constraints ( $s$  and  $\Delta$ ) and in MD simulation with a fixed inorganic part ( $s_f$  and  $\Delta_f$ ) for the studied perovskite materials

	$s$	$s_f$	$\Delta$ (Å)	$\Delta_f$ (Å)
MAPbI <sub>3</sub>	1.59	2.29	0.52	0.66
MAPbBr <sub>3</sub>	1.37	2.25	0.55	0.58
MAPbCl <sub>3</sub>	1.77	2.03	0.55	0.52
MASnI <sub>3</sub>	1.56	2.17	0.50	0.62
FAPbI <sub>3</sub>	1.78	2.40	0.71	0.65
NH <sub>4</sub> PbI <sub>3</sub>	N/A	N/A	0.48	1.11



**Fig. 3** The distribution of orientations of a CN vector for the studied MA-based perovskite materials in MD simulations without constraints and the simulation with a fixed inorganic part.

the case of NH<sub>4</sub>PbI<sub>3</sub>. This departure occurs due to the fact that a NH<sub>4</sub><sup>+</sup> cation has no dipole moment.

Next, we discuss the trends that arise with substitution of halide anions, metal cations or organic cations. To understand these trends we present in Table 3 the rotational entropy and the mean square displacements that quantify the degree of translational motion. In Fig. 3 we present the function  $f(\theta, \phi)$  that also quantifies the degree of rotational freedom of an MA cation.

### Halide anion substitution

In the sequence MAPbCl<sub>3</sub>, MAPbBr<sub>3</sub>, MAPbI<sub>3</sub> the effects of thermal disorder decrease (see the values of  $\sigma(E_g)$  in Table 2) and are in-line with the trend arising from the change of lattice constant. In addition, the rotational flexibility of MAPbCl<sub>3</sub> is the largest in the sequence (see the values for  $s$  in Table 3), which also suggests that it should have the largest thermal disorder. Translational motion of the organic cations is similar

in all three materials (see the values for  $\Delta$  in Table 3) and does not contribute to the differences in band gap variations.

### Metal cation substitution

MASnI<sub>3</sub> has somewhat larger variations of the band gap than MAPbI<sub>3</sub> (see the values of  $\sigma(E_g)$  in Table 2). This difference may arise from the slightly smaller lattice constant of MASnI<sub>3</sub>. On the other hand, rotational and translational motion is slightly larger in MAPbI<sub>3</sub> ( $s$  and  $\Delta$  in Table 3). Nevertheless, due to small differences in the results for the two materials, it is difficult to reliably explain them.

### Organic cation substitution

In the NH<sub>4</sub>PbI<sub>3</sub>, MAPbI<sub>3</sub>, FAPbI<sub>3</sub> sequence, the smallest effects of thermal disorder arise for NH<sub>4</sub>PbI<sub>3</sub> (see  $\sigma(E_g)$  in Table 2). The reasons for this are that NH<sub>4</sub><sup>+</sup> has no dipole moment and it has the smallest translational freedom (smallest  $\Delta$  in Table 3). On the other hand, FAPbI<sub>3</sub> has slightly larger effects of thermal disorder than MAPbI<sub>3</sub> mainly due to larger translational freedom of the organic cation (compare the values of  $\Delta$  in Table 3).

Our aim is also to understand pure effects of organic cations on the electronic properties of the material quantified by band gap variations. To this end, we performed simulations where the inorganic part is fixed. If the degree of rotational and translational freedom of the organic part in such simulations was the same as in the simulations without any constraints, then such simulations would provide information about the effect of the organic cation on the electronic properties of the material. Interestingly, we find that the conformational rotational entropy of organic cations is larger in simulations with a fixed inorganic part, as can be seen from the fact that  $s_f > s$  in Table 3 and from the more smeared dependence  $f(\theta, \phi)$  in the right part of Fig. 3. Such a result can be rationalized by taking into account that the motion of inorganic atoms can occasionally introduce barriers for organic cation rotation that are otherwise not present when inorganic atoms are fixed. As a consequence of larger rotational freedom of organic cations in simulations with fixed inorganic parts, the results of these simulations overestimate the effect of the organic cation on band gap variations in the real material. Therefore, the standard deviation of the band gap obtained from these simulations, that we discuss next, should be considered as the upper limit for the contribution of the organic cation to the band gap variation in the real material.

The trends obtained in simulations with fixed inorganic atoms can be rationalized as follows.

### Halide anion substitution

We find that in the sequence MAPbCl<sub>3</sub>, MAPbBr<sub>3</sub>, MAPbI<sub>3</sub>, the result for MAPbI<sub>3</sub> departs from the trend expected from values of the lattice constants. MAPbI<sub>3</sub> has the largest translational freedom of the organic cation (largest  $\Delta_f$ ) and somewhat larger rotational freedom (largest  $s_f$ ) than the other two materials, leading to larger band gap variations than those expected simply from the lattice constant trend.

### Metal cation substitution

MAPbI<sub>3</sub> has somewhat larger translational and rotational freedom of the organic cation (larger  $s_f$  and  $\Delta_f$ ) than MASnI<sub>3</sub>, which partially explains the larger band gap variations in MAPbI<sub>3</sub>.

### Organic cation substitution

MAPbI<sub>3</sub> has the largest band gap variations due to the largest dipole moment of the organic cation. Although the organic ammonium cation in NH<sub>4</sub>PbI<sub>3</sub> has no dipole moment, it has by far the largest translational freedom (largest  $\Delta_f$ ), which appears to be the reason for the larger band gap variations in NH<sub>4</sub>PbI<sub>3</sub> compared to FAPbI<sub>3</sub>.

Our results indicate that band gap variations in simulations with fixed inorganic atoms are significantly smaller than in simulations without constraints. Taking into account that these band gap variations actually overestimate the effect of the organic cation in the material, we can conclude that the contribution of the organic cation to thermal disorder in electronic properties is much smaller than the contribution of motion of halide and metal atoms. Consequently, to a good approximation, one can think that these materials have similar properties as inorganic semiconductors, although the effects of the organic part cannot be completely neglected. It is also important to point out that this does not mean that substitution of an organic group will lead only to a small change in band gap variations. Namely, the presence of different organic cations in the two materials leads also to different motion of the inorganic part which may also significantly contribute to differences in band gap variations.

Finally, we make some comments on the implications of the effects of thermal disorder on charge carrier mobility in the material. Relevant energy scales that should be used to compare different materials are the (conduction or valence) bandwidth and standard deviation of the band gap or the (conduction or valence) band edge. Namely, when the standard deviation of the band gap becomes comparable to the bandwidth, (dynamical) localization of carriers takes place which significantly slows down the transport. On the other hand, when the bandwidth is much larger than the standard deviation of the band gap the carriers are delocalized and carrier mobility is high. In this work, we found that standard deviation of the band gap in the investigated perovskites falls within the range exhibited in inorganic semiconductors being larger than in non-polar Si, but smaller than in polar GaAs. Band edge variations in ordered regions in organic semiconductors are also of similar order<sup>36,38</sup> as in perovskites or inorganic semiconductors. However, these three groups of semiconductors exhibit quite different charge carrier mobilities. Inorganic Si or GaAs may have mobilities even larger than  $\sim 1000 \text{ cm}^2 \text{ V}^{-1} \text{ s}^{-1}$ , while organic semiconductors rarely exhibit mobilities beyond  $\sim 1 \text{ cm}^2 \text{ V}^{-1} \text{ s}^{-1}$ . The essential difference between these two groups of materials is that bandwidths in inorganic semiconductors are much larger than band edge variations, while in organic semiconductors band edge variations are comparable to bandwidths, leading to strong effects of thermal disorder and

poor charge carrier transport. Halide perovskites exhibit bandwidths somewhat smaller or comparable to the bandwidths of inorganic semiconductors and we have established in this work that band edge variations in the investigated perovskites are comparable to those in inorganic semiconductors. As a consequence, it is expected that organic/inorganic halide perovskites should exhibit similar or somewhat smaller mobilities than inorganic semiconductors. The fact that mobilities beyond  $\sim 100 \text{ cm}^2 \text{ V}^{-1} \text{ s}^{-1}$  were observed in perovskites<sup>72</sup> is consistent with this expectation.

## 4 Conclusions

In conclusion, we investigated in detail the effects of thermal disorder on the electronic properties of organic/inorganic halide perovskite semiconductors. We find that the trend in the strength of thermal disorder can be largely rationalized by considering only the lattice constant of the material. To understand the departure from the main trend one has to take into account the strength of the dipole of the organic cation or the degree of its rotational or translational flexibility. We find that the contribution of the organic cation to band gap variations is considerably smaller than the contribution of the inorganic part. The strength of these variations, as well as the bandwidths of the material, are similar as in inorganic semiconductors, in agreement with very good charge transport properties of halide perovskites.

## Conflicts of interest

There are no conflicts to declare.

## Acknowledgements

We gratefully acknowledge the support by the Ministry of Education, Science and Technological Development of the Republic of Serbia (Project No. ON171017) and the European Commission under H2020 project VI-SEEM, Grant No. 675121, and contribution of the COST Action MP1406. Numerical computations were performed on the PARADOX supercomputing facility at the Scientific Computing Laboratory of the Institute of Physics Belgrade.

## References

- 1 J.-P. Correa-Baena, M. Saliba, T. Buonassisi, M. Grätzel, A. Abate, W. Tress and A. Hagfeldt, *Science*, 2017, **358**, 739–744.
- 2 Q. Chen, N. D. Marco, Y. M. Yang, T.-B. Song, C.-C. Chen, H. Zhao, Z. Hong, H. Zhou and Y. Yang, *Nano Today*, 2015, **10**, 355–396.
- 3 M. M. Lee, J. Teuscher, T. Miyasaka, T. N. Murakami and H. J. Snaith, *Science*, 2012, **338**, 643–647.
- 4 M. Liu, M. B. Johnston and H. J. Snaith, *Nature*, 2013, **501**, 395–398.

- 5 M. A. Green, Y. Hishikawa, E. D. Dunlop, D. H. Levi, J. Hohl-Ebinger and A. W. Ho-Baillie, *Prog. Photovoltaics*, 2018, **26**, 3–12.
- 6 W.-J. Yin, J.-H. Yang, J. Kand, Y. Yan and S.-H. Wei, *J. Mater. Chem. A*, 2015, **3**, 8926–8942.
- 7 J. Even, L. Pedesseau, C. Katan, M. Kepenekian, J.-S. Lauret, D. Saponi and E. Deleporte, *J. Phys. Chem. C*, 2015, **119**, 10161–10177.
- 8 L. D. Whalley, J. M. Frost, Y.-K. Jung and A. Walsh, *J. Chem. Phys.*, 2017, **146**, 220901.
- 9 W. Geng, L. Zhang, Y.-N. Zhang, W.-M. Lau and L.-M. Liu, *J. Phys. Chem. C*, 2014, **118**, 19565–19571.
- 10 A. Mattoni, A. Filippetti and C. Caddeo, *J. Phys.: Condens. Matter*, 2017, **29**, 043001.
- 11 S. Meloni, G. Palermo, N. Ashari-Astani, M. Grätzel and U. Rothlisberger, *J. Mater. Chem. A*, 2016, **4**, 15997–16002.
- 12 M. R. Filip and F. Giustino, *Phys. Rev. B: Condens. Matter Phys.*, 2014, **90**, 245145.
- 13 S. X. Tao, X. Cao and P. A. Bobbert, *Sci. Rep.*, 2017, **7**, 14386.
- 14 E. Mosconi, C. Quarti, T. Ivanovska, G. Ruani and F. De Angelis, *Phys. Chem. Chem. Phys.*, 2014, **16**, 16137–16144.
- 15 M. A. Carignano, A. Kachmar and J. Hutter, *J. Phys. Chem. C*, 2015, **119**, 8991–8997.
- 16 J. M. Frost, K. T. Butler and A. Walsh, *APL Mater.*, 2014, **2**, 081506.
- 17 A. Mattoni, A. Filippetti, M. I. Saba and P. Delugas, *J. Phys. Chem. C*, 2015, **119**, 17421–17428.
- 18 M. T. Weller, O. J. Weber, J. M. Frost and A. Walsh, *J. Phys. Chem. Lett.*, 2015, **6**, 3209–3212.
- 19 A. A. Bakulin, O. Selig, H. J. Bakker, Y. L. Rezus, C. Müller, T. Glaser, R. Lovrincic, Z. Sun, Z. Chen, A. Walsh, J. M. Frost and T. L. C. Jansen, *J. Phys. Chem. Lett.*, 2015, **6**, 3663–3669.
- 20 C. Quarti, E. Mosconi and F. De Angelis, *Phys. Chem. Chem. Phys.*, 2015, **17**, 9394–9409.
- 21 J. M. Frost and A. Walsh, *Acc. Chem. Res.*, 2016, **49**, 528–535.
- 22 C. Quarti, E. Mosconi, J. M. Ball, V. D’Innocenzo, C. Tao, S. Pathak, H. J. Snaith, A. Petrozza and F. De Angelis, *Energy Environ. Sci.*, 2016, **9**, 155–163.
- 23 A. L. Montero-Alejo, E. Menéndez-Proupin, D. Hidalgo-Rojas, P. Palacios, P. Wahnón and J. C. Conesa, *J. Phys. Chem. C*, 2016, **120**, 7976–7986.
- 24 J. Even, M. Carignano and C. Katan, *Nanoscale*, 2016, **8**, 6222–6236.
- 25 M. A. Carignano, Y. Saeed, S. A. Aravindh, I. S. Roqan, J. Even and C. Katan, *Phys. Chem. Chem. Phys.*, 2016, **18**, 27109–27118.
- 26 J. Lahnsteiner, G. Kresse, A. Kumar, D. D. Sarma, C. Franchini and M. Bokdam, *Phys. Rev. B*, 2016, **94**, 214114.
- 27 O. Selig, A. Sadhanala, C. Müller, R. Lovrincic, Z. Chen, Y. L. A. Rezus, J. M. Frost, T. L. C. Jansen and A. A. Bakulin, *J. Am. Chem. Soc.*, 2017, **139**, 4068–4074.
- 28 M. A. Carignano, S. A. Aravindh, I. S. Roqan, J. Even and C. Katan, *J. Phys. Chem. C*, 2017, **121**, 20729–20738.
- 29 O. Yaffe, Y. Guo, L. Z. Tan, D. A. Egger, T. Hull, C. C. Stoumpos, F. Zheng, T. F. Heinz, L. Kronik, M. G. Kanatzidis, J. S. Owen, A. M. Rappe, M. A. Pimenta and L. E. Brus, *Phys. Rev. Lett.*, 2017, **118**, 136001.
- 30 C. Goehry, G. A. Nemnes and A. Manolescu, *J. Phys. Chem. C*, 2015, **119**, 19674–19680.
- 31 J. Ma and L.-W. Wang, *Nano Lett.*, 2015, **15**, 248–253.
- 32 J. Kang and L.-W. Wang, *J. Phys. Chem. Lett.*, 2017, **8**, 3875–3880.
- 33 S. Kanno, Y. Imamura, A. Saeki and M. Hada, *J. Phys. Chem. C*, 2017, **121**, 14051–14059.
- 34 S. Kanno, Y. Imamura and M. Hada, *J. Phys. Chem. C*, 2017, **121**, 26188–26195.
- 35 T. Chen, B. J. Foley, B. Ipek, M. Tyagi, J. R. D. Copley, C. M. Brown, J. J. Choi and S.-H. Lee, *Phys. Chem. Chem. Phys.*, 2015, **17**, 31278–31286.
- 36 A. Troisi and G. Orlandi, *Phys. Rev. Lett.*, 2006, **96**, 086601.
- 37 S. Fratini and S. Ciuchi, *Phys. Rev. Lett.*, 2009, **103**, 266601.
- 38 M. Mladenović and N. Vukmirović, *Phys. Chem. Chem. Phys.*, 2014, **16**, 25950–25958.
- 39 M. Mladenović and N. Vukmirović, *Adv. Funct. Mater.*, 2015, **25**, 1915–1932.
- 40 T. Vehoff, B. Baumeier, A. Troisi and D. Andrienko, *J. Am. Chem. Soc.*, 2010, **132**, 11702–11708.
- 41 J. Böhlin, M. Linares and S. Stafström, *Phys. Rev. B: Condens. Matter Mater. Phys.*, 2011, **83**, 085209.
- 42 A. Troisi and D. L. Cheung, *J. Chem. Phys.*, 2009, **131**, 014703.
- 43 A. Troisi, *J. Chem. Phys.*, 2011, **134**, 034702.
- 44 Y. Yao, W. Si, X. Hou and C.-Q. Wu, *J. Chem. Phys.*, 2012, **136**, 234106.
- 45 D. L. Cheung, D. P. McMahon and A. Troisi, *J. Am. Chem. Soc.*, 2009, **131**, 11179–11186.
- 46 T. Liu and A. Troisi, *Adv. Funct. Mater.*, 2014, **24**, 925–933.
- 47 S. Fratini, S. Ciuchi, D. Mayou, G. T. de Laissardière and A. Troisi, *Nat. Mater.*, 2017, **16**, 998.
- 48 S. Baroni, S. de Gironcoli, A. Dal Corso and P. Giannozzi, *Rev. Mod. Phys.*, 2001, **73**, 515–562.
- 49 F. Giustino, *Rev. Mod. Phys.*, 2017, **89**, 015003.
- 50 E. Mosconi, J. M. Azpiroz and F. De Angelis, *Chem. Mater.*, 2015, **27**, 4885–4892.
- 51 P. Giannozzi, S. Baroni, N. Bonini, M. Calandra, R. Car, C. Cavazzoni, D. Ceresoli, G. L. Chiarotti, M. Cococcioni, I. Dabo, A. Dal Corso, S. de Gironcoli, S. Fabris, G. Fratesi, R. Gebauer, U. Gerstmann, C. Gougoussis, A. Kokalj, M. Lazzeri, L. Martin-Samos, N. Marzari, F. Mauri, R. Mazzarello, S. Paolini, A. Pasquarello, L. Paulatto, C. Sbraccia, S. Scandolo, G. Sclauzero, A. P. Seitsonen, A. Smogunov, P. Umari and R. M. Wentzcovitch, *J. Phys.: Condens. Matter*, 2009, **21**, 395502.
- 52 P. Giannozzi, O. Andreussi, T. Brumme, O. Bunau, M. B. Nardelli, M. Calandra, R. Car, C. Cavazzoni, D. Ceresoli, M. Cococcioni, N. Colonna, I. Carnimeo, A. D. Corso, S. de Gironcoli, P. Delugas, R. A. D. Jr, A. Ferretti, A. Floris, G. Fratesi, G. Fugallo, R. Gebauer, U. Gerstmann, F. Giustino, T. Gorni, J. Jia, M. Kawamura, H.-Y. Ko, A. Kokalj, E. Kucukbenli, M. Lazzeri, M. Marsili, N. Marzari, F. Mauri, N. L. Nguyen, H.-V. Nguyen, A. O. de-la Roza, L. Paulatto, S. Poncé, D. Rocca, R. Sabatini, B. Santra, M. Schlipf, A. P. Seitsonen, A. Smogunov, I. Timrov, T. Thonhauser, P. Umari, N. Vast, X. Wu and S. Baroni, *J. Phys.: Condens. Matter*, 2017, **29**, 465901.

- 53 <https://github.com/WMD-group/hybrid-perovskites>.
- 54 F. Brivio, A. B. Walker and A. Walsh, *APL Mater.*, 2013, **1**, 042111.
- 55 F. Brivio, K. T. Butler, A. Walsh and M. van Schilfgaarde, *Phys. Rev. B: Condens. Matter Mater. Phys.*, 2014, **89**, 155204.
- 56 C. C. Stoumpos, C. D. Malliakas and M. G. Kanatzidis, *Inorg. Chem.*, 2013, **52**, 9019–9038.
- 57 J. P. Perdew, M. Ernzerhof and K. Burke, *J. Chem. Phys.*, 1996, **105**, 9982–9985.
- 58 C. Adamo and V. Barone, *J. Chem. Phys.*, 1999, **110**, 6158–6170.
- 59 S. Grimme, *J. Comput. Chem.*, 2006, **27**, 1787–1799.
- 60 F. Chen, C. Zhu, C. Xu, P. Fan, F. Qin, A. Gowri Manohari, J. Lu, Z. Shi, Q. Xu and A. Pan, *J. Mater. Chem. C*, 2017, **5**, 7739–7745.
- 61 M. Sendner, P. K. Nayak, D. A. Egger, S. Beck, C. Muller, B. Epping, W. Kowalsky, L. Kronik, H. J. Snaith, A. Pucci and R. Lovrincic, *Mater. Horiz.*, 2016, **3**, 613–620.
- 62 M. T. Weller, O. J. Weber, P. F. Henry, A. M. Di Pumpo and T. C. Hansen, *Chem. Commun.*, 2015, **51**, 4180–4183.
- 63 R. Wasylshen, O. Knop and J. Macdonald, *Solid State Commun.*, 1985, **56**, 581–582.
- 64 G. R. Berdiyrov, A. Kachmar, F. El-Mellouhi, M. A. Carignano and M. E.-A. Madjet, *J. Phys. Chem. C*, 2016, **120**, 16259–16270.
- 65 A. M. A. Leguy, P. Azarhoosh, M. I. Alonso, M. Campoy-Quiles, O. J. Weber, J. Yao, D. Bryant, M. T. Weller, J. Nelson, A. Walsh, M. van Schilfgaarde and P. R. F. Barnes, *Nanoscale*, 2016, **8**, 6317–6327.
- 66 S. Pang, H. Hu, J. Zhang, S. Lv, Y. Yu, F. Wei, T. Qin, H. Xu, Z. Liu and G. Cui, *Chem. Mater.*, 2014, **26**, 1485–1491.
- 67 P. Umari, E. Mosconi and F. De Angelis, *Sci. Rep.*, 2014, **4**, 4467.
- 68 J. Wiktor, U. Rothlisberger and A. Pasquarello, *J. Phys. Chem. Lett.*, 2017, **8**, 5507–5512.
- 69 J. Kohanoff, *Electronic Structure Calculations for Solids and Molecules: Theory and Computational Methods*, Cambridge University Press, 2006.
- 70 C. Motta, F. El-Mellouhi, S. Kais, N. Tabet, F. Alharbi and S. Sanvito, *Nat. Commun.*, 2015, **6**, 7026.
- 71 D. A. Egger and L. Kronik, *J. Phys. Chem. Lett.*, 2014, **5**, 2728–2733.
- 72 L. M. Herz, *ACS Energy Lett.*, 2017, **2**, 1539–1548.